Extraction of particle size via Fourier ptychography with selective illuminations

Li Shengfu, Zhao Yu, Chen Guanghua, Luo Zhenxiong, Ye Yan

(Institute of Fluid Physics, China Academy of Engineering Physics, Mianyang 621900, China)

Abstract: A method, which can extract the particle size information with a resolution beyond λ/NA, was proposed. This was achieved by applying Fourier ptychographic (FP) ideas to the present problem. In a typical FP imaging platform, a 2D LED array was used as light sources for angle-varied illuminations, a series of low-resolution images were taken by a full sequential scan of the array of LEDs, and the data were then combined to produce a high-resolution image. Here, the particle size information was extracted by turning on each single LED on a circle, whose radius was chosen according to an expression for the resolution limit. The simulated results show that the proposed method can reduce the total number of images without loss of reliability in the results, and the total number of images can be further reduced by optimizing the aperture overlapping rate.

Key words: dark field; computational imaging; particle size; microscopy

CLC number: O438.2 **Document code:** A **DOI:** 10.3788/IRLA201746.1103005

选择型照明傅里叶叠层成像提取粒子尺度

李生福,赵 宇,陈光华,罗振雄,叶 雁

(中国工程物理研究院流体物理研究所,四川 绵阳 621900)

摘 要: 提出了一种粒子尺度信息提取方法, 通过将傅里叶叠层思想应用到粒子尺度信息提取中实现了比 λ/NA 更高的空间分辨率。在传统的傅里叶叠层成像系统中,采用一个二维 LED 阵列作为光源以获得不同角度的照明,通过扫描阵列中的所有 LED,获取一系列低分辨图像,然后利用这些低分辨图像生成一幅高分辨图像。为了减少所需的低分辨图像幅数,进一步提出了选择型照明傅里叶叠层成像提取粒子尺度信息的方法,通过分布在一个圆周上的 LED 提取粒子尺度信息,根据分辨率极限公式给出了圆周半径的选择方法。仿真结果结果表明提出的方法在不损失精度的前提下能够大幅度减少需要的低分辨图像幅数。

关键词: 暗场; 计算成像; 粒子尺度; 显微镜

收稿日期: 2017-09-05; **修订日期:** 2017-11-03

基金项目: 国家自然科学基金(11702275,11672275);科学挑战计划(TZ2016001)

作者简介: 李生福(1984-),助理研究员,博士,主要从事高分辨成像、数字全息和光声成像方面的研究。Email:lisfu2008@163.com

0 Introduction

The problem of extracting the particle size information is particularly important in diverse fields[1-5]. Many methods for particle size estimation[1] have been proposed in published papers[6-10]. Essentially, these methods obtain the particle size information by employing forward propagation through Fourier methods and digital image processing methods such as pixel counting. Thus, the finite CCD pixel size influence the estimation precision, especially for particle diameters less than the pixel size.

Considering that Fourier Ptychographic (FP) methods[11-14] can overcome the limit of the finite CCD pixel size and thus can improve the estimation precision, this paper applies FP methods to the present problem. FP methods have been widely investigated and its in-principle advantages can be found and understood in associated references. In a typical FP imaging platform, a 2D LED array is used as light sources for angle-varied illuminations, a series of low-resolution images was taken by a full sequential scan of the array of LEDs, and the data were then combined to produce a high-resolution image. Usually, a high-resolution image is produced by scanning through each of the LEDs in the array, leading to hundreds of images in each dataset. Thus, the main limitations of typical Fourier ptychography are the large amount of data captured and the long acquisition times required.

In the present paper, we propose a FP method which can extract the particle size information from fewer images (less than 20 images) by eliminating redundancy in the data. The approach is inspired by the Archimedes′ method[15]: the area of the unit circle can be approximated with inscribed and circumscribed polygons of N sides. This indicates that one only needs to acquire the information corresponding to particle edges and treats other as redundancy, and thus provides the feasibility to extract the particle size information from fewer images. Our method combines FP methods and Archimedes′ ideas to extract the particle size information from fewer images.

1 Method

1.1 Fourier ptychography

The principle of Fourier ptychography is illustrated in Fig.1. The sample(Particles) is located in the object plane, with coordinates x and y, and a recording is performed in the recording plane, with coordinates ξ and η. In a typical FP imaging platform, a 2D LED array is used as light sources for angle-varied illuminations, a series of low-resolution images was taken by a full sequential scan of the array of LEDs. Let $o(x,y)$ be the complex scalar transmission profile of the sample, and the illumination wave generated by an arbitrary LED be plane and have polar angle θ and azimuthal angle φ. The complex scalar field of the transmitted wave is given by

$$o(x,y)\mathrm{e}^{i(f_{x0}x+f_{y0}y)} \tag{1}$$

where,

$$f_{x0}=\frac{\sin\theta\cos\varphi}{\lambda}$$
$$f_{y0}=\frac{\sin\theta\sin\varphi}{\lambda} \tag{2}$$

and λ is the wavelength of light. The Fourier transform of $o(x,y)$ is noted by $O(k_x,k_y)$.

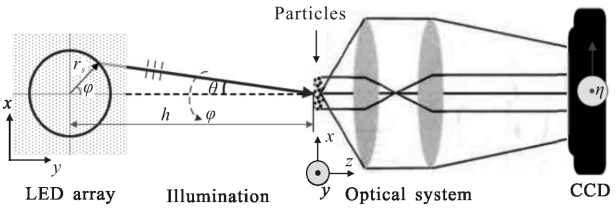

Fig.1 Principle of Fourier ptychography

As explained in reference[11], the resolution can be improved by using oblique illumination as shown in Fig.1, providing an effective numerical aperture(NA)

$$\mathrm{NA}_{\mathrm{eff}}=\mathrm{NA}+\sin\theta \tag{3}$$

1.2 Determination of particle size with polygons

Archimedes [15] approximated the area of a unit circle inscribed and circumscribed polygons of N

sides. As N approaches infinity, the two polygonal areas should approach the area of the unit circle, as shown in Fig.2, where Fig.2(a) shows that the size of a circle with a radius of r can be approximated with a circumscribed polygon of four sides. This idea point can also be extended to non-spherical particles, as shown in Fig.3.

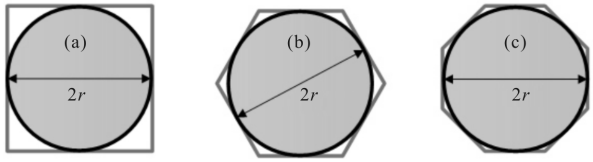

Fig.2 Determination of the area of a unit circle (spherical particle) using polygons

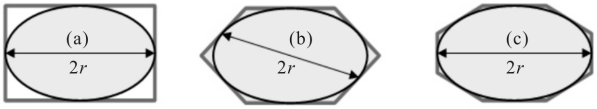

Fig.3 Determination of the area of a non-spherical particle using polygons

1.3 Particle edges in the Fourier domain

In the Fourier domain, edges correspond to the high frequency components[16]. This also holds for particles and can be easily confirmed by a simple simulation, as shown in Fig.4, where Fig.4(a) shows a simulated object which consists of particles. A high-pass filtering process is performed, as shown in Fig.4(b), where we transform the object′s intensity to the spatial-frequency domain using fast Fourier transform and multiply it with the high-pass filter. The final high-pass filtered intensity output is in Fig.4(c).

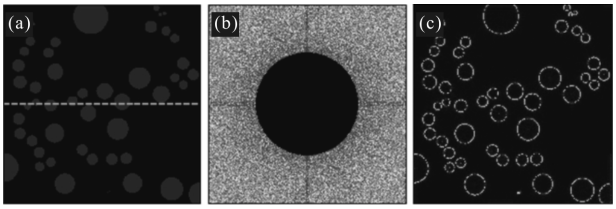

Fig.4 (a) A simulated particle field; (b) performing a high-pass filtering process; (c) final high-pass filtered intensity output

1.4 Acquisition of information corresponding to particle edges

Figures 2 and 3 show that the size of a particle can be determined by its edges (even via a circumscribed polygon). Thus, to extract particle size only needs to acquire the information corresponding to particle edges and treat other as redundancy. Figure 4 shows that particle edges correspond to the high frequency components in the Fourier domain. We eliminate the redundancy by turning on each single LED on a circle with a radius of rs, as shown in Fig.5. Evidently, r_s should be determined by the required resolution $r_{\min}$. Considering that, in this present paper, we try to extract the particle size information from particle edges, thus rmin should be chosen as the minimum diameter, as d in Fig.5. Note that it is different from the minimum center-to-center distance, which is usually used to define the resolution of microscopy, as R_O in Fig.5.

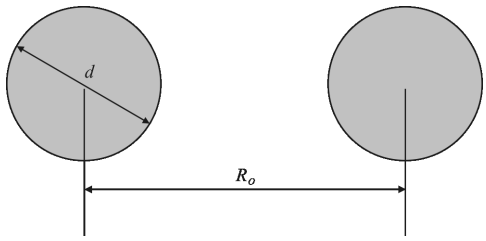

Fig.5 Definition of $r_{\min}$

According to Eq.(3), d can be expressed as,

$$d=\frac{\lambda}{\text{factor}\cdot\text{NA}+\sin(\theta)} \tag{4}$$

The illumination wave generated by the LEDs on the circle has a fixed polar angle, noted by θ_p. From Eq.(4), one can obtain,

$$\sin(\theta_p)=\frac{\lambda}{d}-\text{factor}\cdot\text{NA} \tag{5}$$

From Fig.1, have,

$$\sin(\theta_p)=\frac{h}{\sqrt{h^2+r_s^2}} \tag{6}$$

then,

$$r_s=\frac{h}{\sqrt{1-(\lambda/2d-\text{factor}\cdot\text{NA})}} \tag{7}$$

where, factor is a positive real number and meets the following equation: 0<factor<1.

Suppose that circumscribed polygons of 2N sides

are employed to extract the particle size information, then the corresponding azimuthal angle φ_k has the form

$$\varphi_k=\varphi_0+k\frac{\pi}{N},\ k=1,\ 2,\ \cdots,\ N-1 \tag{8}$$

1.5 Reconstruction

The goal of the reconstruction procedure is to recover the function of $O(k_x,k_y)$ by using an iterative approach. Let I_k be the captured low-resolution images under angularly varying illumination, where k has been defined before. The reconstruction procedure starts from an initial guess of the function $O_g(k_x,k_y)$. The notation $O_s^{(j)}(k_x,k_y)$ is the sample function in the j_{th} loop. According to Eq.(1), Eq.(5) and Eq.(8), a sub-region is selected from the sample function and converted into the spatial domain, producing the simulated image:

$$\sqrt{I_{s,k}}\,e^{i\varphi_s}=F^{-1}\{O_g^{(j)}(k_x-k_{xN},k_y-k_{yN})\cdot P\} \tag{9}$$

with,

$$k_{xN}=\frac{\sin\theta_P}{\lambda}\cos\left(\varphi_0+k\frac{\pi}{N}\right)$$

$$k_{yN}=\frac{\sin\theta_P}{\lambda}\sin\left(\varphi_0+k\frac{\pi}{N}\right)$$

P is the pupil function of the imaging system. The amplitude of the simulated image is replaced with the square root of I_k, obtaining the corrected image

$$\sqrt{I_k}\,e^{i\varphi_s} \tag{10}$$

Then, the corrected image is converted into the Fourier domain and updates its corresponding sub-region of the sample function

$$O_g^{(j+1)}(k_x,k_y)=P^*\cdot F(\sqrt{I_k}\,e^{i\varphi_s}) \tag{11}$$

To implement an iteration, one needs to repeat Eq. (9) to Eq. (11) for different incident angles. In fact, multiple iterations are required to obtain a solution with a certain precision.

2 Simulations

Several examples are provided to demonstrate the above method by recovering particle edges from simulated measurements. The numerical sample was produced by randomly choosing particle positions based on a pseudo-random number generator[17]. The numerical phantom has been given in Fig.4 (a). Measurements were simulated using Eq.(12)

$$M_k=|F^{-1}\{O(k_x-k_{xN},k_y-k_{yN})\}\cdot P| \tag{12}$$

where, P represents the pupil function of the imaging system.

The optical system was modeled by a low-pass filter with a cutoff frequency of NA/λ, NA represents the numerical aperture of the objective lens. The incident wavelength was taken as 0.532 μm. For each example, the desired resolution was taken as the minimum particle diameter and fixed a value of θ_p by use of Eq.(5).

2.1 Extraction from noise-free data

The first example, which consisted of 50 particles with diameters ranging from 0.75 μm to 67.5 μm, within a transparent medium, is shown in Fig.4 (a). The desired resolution is 0.75 μm and the resolved $\sin(\theta_p)$ is 0.5; N and NA were taken as 16 and 0.22, respectively. Following 100 iterations of the reconstruction procedure, the recovered results were obtained and are shown in Fig.6, where Fig.6(a) shows the recovered Fourier spectrum, and Fig.6(b) is the recovered intensity. Figure 6(b) show that the particle edges have been recovered well. Note in the present paper, the recovered results are shown in log-scale.

Theoretically, $\sin(\theta_p)$ can also be taken as a value greater than 0.5. Figures 7(a) and (b) respectively show the recovered Fourier spectrum and intensity corresponding to $\sin(\theta_p)$=0.75. From the regions marked by rectangles in Fig.6(b) and Fig.7(b), it can be seen that the increase in $\sin(\theta_p)$ leads to a decrease in the image contrast. This is due to the fact that the spatial spectrum exhibits monotonously decreasing trends along the radial direction. To optimize the image contrast, it is not enough only to consider Eq.(5), the spatial spectrum must be accounted for as well.

We also finished simulations for $\sin(\theta_p)$ being less than 0.5. Figures 8(a) and (b) respectively show the recovered Fourier spectrum and intensity corresponding to $\sin(\theta_p)$=0.25. From the regions marked

by rectangles in Fig.6(b), Fig.7(b) and Fig.8(b), it can be seen that one should try to choose $\sin(\theta_p)$ according to Eq.(5).

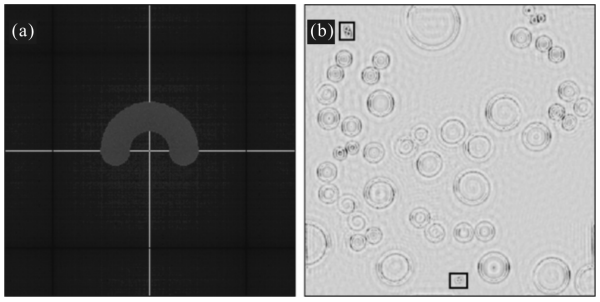

Fig.6 Recovered Fourier spectrum (a) and intensity (b) (Particle edge extraction with $\sin(\theta_p)$=0.5)

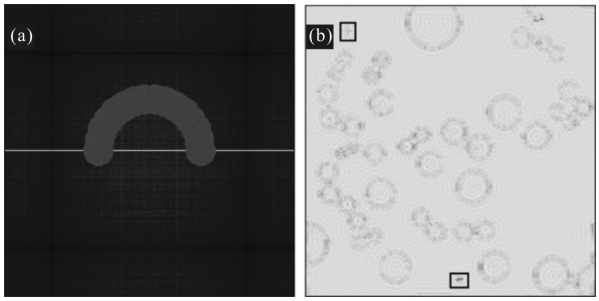

Fig.7 Recovered Fourier spectrum (a) and intensity (b) (Particle edge extraction with $\sin(\theta_p)$=0.75)

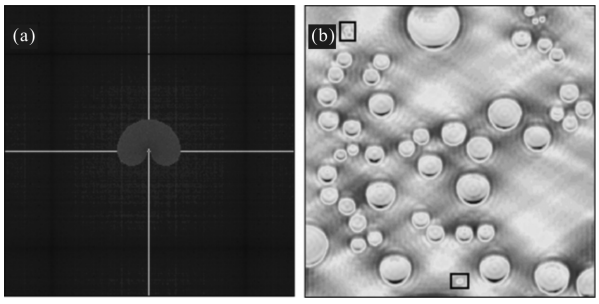

Fig.8 Recovered Fourier spectrum (a) and intensity (b) (Particle edge extraction with $\sin(\theta_p)$=0.25)

2.2 Extraction from noisy data

The simulations in Subsection 2.1 show that the proposed method can be used to obtain an accurate, quantitative estimate of the particle size from noise-free data. However, employing exactly the same model for the measurements and the reconstruction is considered an inverse crime. To avoid this inverse crime, noise was added to the simulated data in this Subsection, as shown in Eq.(13), $k_{x,r}$ and $k_{y,r}$ represents the wavenumber used in the reconstruction procedure.

$$k_{x,r}=k_x+\delta_x$$
$$k_{y,r}=k_y+\delta_y \quad (13)$$

Figures 9(a) and (b) respectively show the recovered Fourier spectrum and intensity from noisy data, δ_x and δ_y were simulated with a random function. The effects of δ_x and δ_y on the remonstration procedure can be understandable from the distorted circle in Fig.9(a). As reported in Ref.[18], we also improved Fig.9(a) and (b) with recently proposed positional misalignment correction methods, as shown in Fig.9(c) and (d). The success of the reconstruction in Fig.9 further confirms the feasibility of the proposed method.

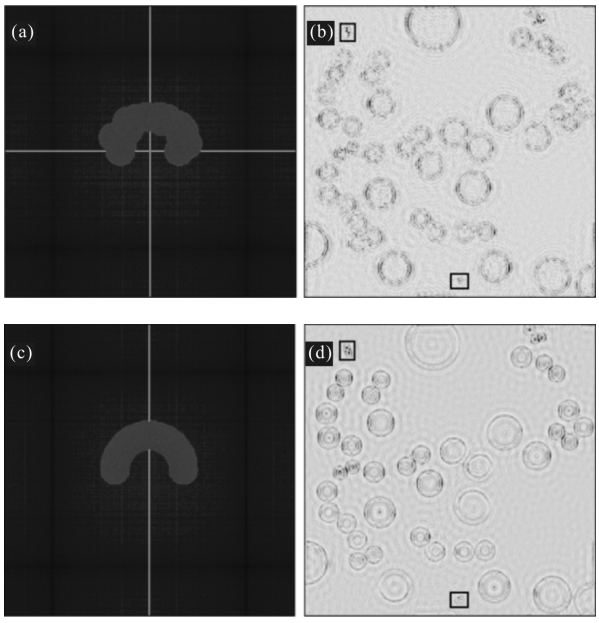

Fig.9 Particle edge extraction from noisy data

2.3 Example for *d* less than λ

The simulation in this Subsection is also based on the sample shown in Fig.4(a). The minimum particle diameter was taken as λ/1.6 and thus d in Eq.(4) equals to λ/1.6. $\sin(\theta_p)$ was taken as 1.2, as in Ref.[19]; NA was taken as 0.42. Figures 10 (a) and (b) respectively show the recovered Fourier spectrum and intensity. The recovered results show that the proposed method can be applied to the particles with *d* less than λ.

The image contrast in Fig.6 to Fig.10 can be simply improved by adding the illumination, θ=0. An example is shown Fig.11, which shows the improved version of Fig.6 and the image contrast has been evidently ameliorated. This is due to the fact that signal energy is concentrated at low-frequencies. The simulations above are based on a numerical phantom consisted of spherical particles (disks). The proposed method is also tested with squares, as show in Fig.12, where Fig.12(a) is a numerical phantom. Measurements were simulated using Eq.(12). The recovered intensity is shown in Fig.12(b). It can be seen from Fig.12 that our method can also be applied to non-spherical particles.

Our method can be considered as a smart version of dark-field FP[20], that is, the angles of oblique illumination are theoretically selected by the desired resolution. The minimum diameter: d in Eq.(5) can be determined by priori information and resolution of interest.

The resolution limit of the proposed method λ/NA_{eff} is much better than that of typical pixel counting methods, λ/NA, the definitions of NA and NA_{eff} have been given before. Thus, the proposed scheme leads to improved accuracy compared to typical pixel counting methods.

Once the particle edge is acquired, the size can be easily obtained by using the Archimedes′ idea or other approaches, such as typical pixel counting methods. It is also noteworthy that the proposed method can be easily extended into 3D applications, though the simulation results are obtained for 2D cases. This is due to the fact that Fourier ptychography has been extended into 3D cases[21]. The simulated results show that our scheme does not have to exhaustively sample Fourier domain as typical FP, and thus can reduce the number of captured images. There is another factor which influences the number of captured images: the aperture-overlapping-rate $R_{overlap}$[22]. Figures 13 (a)−(d) present the recovered intensity images with the $R_{overlap}$ increasing. These results shown in Fig.13 were obtained with the data used in Fig.6. For other simulation experiments, one can obtain a set of similar results. The results shown in Fig.13 indicate that $R_{overlap}$ should be taken as ~45% in our proposed method. If $R_{overlap}$ <45% , the redundancy would be insufficient for accurately recovering the intensity images. By optimizing $R_{overlap}$, only 9 low-resolution images are needed to produce the result shown in Fig.13(d).

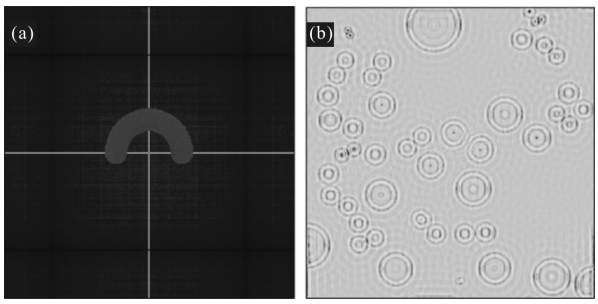

Fig.10 Recovered Fourier spectrum (a) and intensity (b) (Particle edge extraction for r_{min}=λ/1.6)

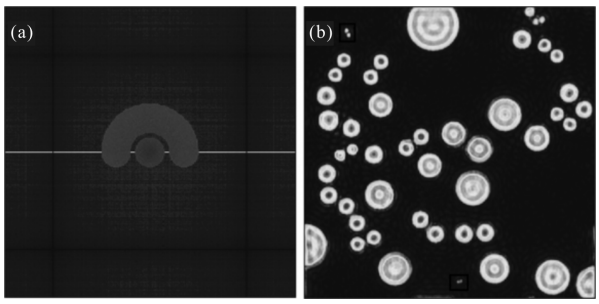

Fig.11 Recovered Fourier spectrum (a) and intensity (b) (Improved version of Fig.6)

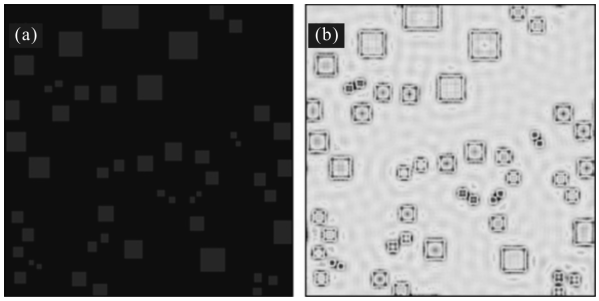

Fig.12 Applying the proposed method to squares, (a) numerical phantom and (b) recovered intensity

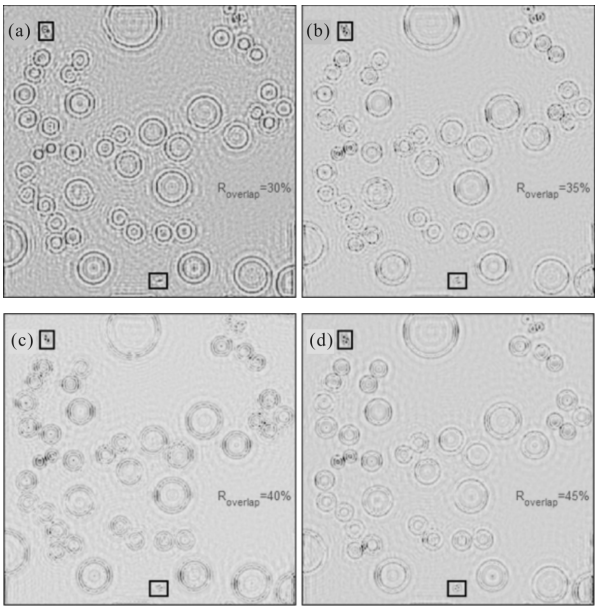

Fig.13 Comparison of the recovery qualities with different aperture-overlapping-rate $R_{overlap}$

3 Conclusion

By exploiting the Archimedes′ ideas, we proposed a FP method which extracts the particle size information from the information corresponding to each single LED distributed along a circle, as shown in Fig.1. The radius of the circle is chosen according to Eq.(4) and Eq.(5). Our method does not have to exhaustively sample Fourier domain as typical FP, and thus can reduce the number of captured images and ease burdens on both storage and processing. The number of captured images is further reduced by optimizing the aperture overlapping rate. The proposed method is validated with noise-free and noisy data. The simulated results show that the proposed leads to improved accuracy compared to typical pixel counting methods.

References:

[1] Jiang Lu, Raymond A S, Yang Weidong. Improved particle size estimation in digital holography via sign matched filtering[J]. ***Opt Express***, 2012, 20(12): 12666-12674.

[2] Katz J, Sheng J. Applications of holography in fluid mechanics and particle dynamics[J]. ***Annu Rev Fluid Mech***, 2012, 42: 531-555.

[3] Fugal J P, Shaw R A. Cloud particle size distributions measured with an airborne digital in-line holographic instrument[J]. ***Atmos Meas Tech***, 2009, 2: 259-271.

[4] Shi Zhenhua, Lin Guanyu, Wang Shurong, et al. Numerical analysis of small particle measurement based on the theory of laser scattering [J]. ***Infrared and Laser Engineering***, 2015, 44(7): 2189-2194. (in Chinese)

[5] Yang Chunling, Zhang Zhendong, Liu Guocheng. Influence of particle radius of composition on radiation characteristics of infrared decoy[J]. ***Infrared and Laser Engineering***, 2016, 45(S1): S104005. (in Chinese)

[6] Denis L, Fournier C, Fournel T, et al. Direct extraction of the mean particle size from a digital hologram[J]. ***Appl Opt***, 2006, 45(5): 944-952.

[7] Pan G, Meng H. Digital holography of particle fields: reconstruction by use of complex amplitude [J]. ***Appl Opt***, 2003, 42(5): 827-833.

[8] Yang W, Kostinski A B, Shaw R A. Depth-of-focus reduction for digital in-line holography of particle fields[J]. ***Opt Lett***, 2005, 30(11): 1303-1305.

[9] Soulez F, Denis L, Fournier C, et al. Inverse problem approach for particle digital holography: accurate location based on local optimisation [J]. ***J Opt Soc Am A***, 2007, 24 (4): 1164-1171.

[10] Dixon L, Cheong F C, Grier D G. Holographic deconvolution microscopy for high-resolution particle tracking [J]. ***Opt Express***, 2011, 19(11): 16410-16417.

[11] Zheng G, Horstmeyer R, Yang C. Wide-field, high-resolution Fourier ptychographic microscopy[J]. ***Nat Photonics***, 2013, 7 (9): 739-745.

[12] Tian L, Li X, Ramchandran K, et al. Multiplexed coded illumination for Fourier ptychography with an LED array microscope[J]. ***Biomed Opt Express***, 2014, 5(7): 2376-2389.

[13] Bian L, Suo J, Situ G, et al. Content adaptive illumination for Fourier ptychography[J]. ***Opt Lett***, 2014, 39(23): 6648-6651.

[14] Ou X, Zheng G, Yang C. Embedded pupil function recovery for Fourier ptychographic microscopy [J]. ***Opt Express***, 2014, 22(5): 4960-4972.

[15] Archimedes. From wikipedia, the free encyclopedia[EB/OL]. (2017-01-01). https://en.wikipedia.org/wiki/Archimedes.

[16] Li Changtsun, Lou Derchyuan. Edge detection based on the multiresolution Fourier transform[C]//IEEE Workshop, Signal

Processing Systems, 1999.

[17] Wang L, Jacques S L, Zheng L Q. MCML-Monte Carlo modeling of lighttransport in multilayered tissues[J]. ***Comput Methods Prog Biomed***, 1995, 47(2): 131-146.

[18] Sun J, Chen Q, Zhang Y, et al. Efficient positional misalignment correction method for Fourier ptychographic microscopy[J]. ***Biomed Opt Express***, 2016, 7(4): 1336.

[19] Sun J, Zuo C, Zhang L, et al. Resolution-enhanced Fourier ptychographic microscopy based on high-numerical-aperture illuminations[J]. ***Scientific Reports***, 2017, 7(1): 1187.

[20] Guo K, Dong S, Zheng G. Fourier ptychography for brightfield, phase, darkfield, reflective, multi-Slice, and fluorescence imaging [J]. ***IEEE Journal of Selected Topics in Quantum Electronics***, 2016, 22(4): 77-88.

[21] Tian L, Waller L. 3D intensity and phase imaging from light field measurements in an LED array microscope [J]. ***Optica***, 2016, 22(7): 104-111.

[22] Sun J, Chen Q, Zhang Y, et al. Sampling criteria for Fourier ptychographic microscopy in object space and frequency space[J]. ***Opt Express***, 2016, 24(14): 15765-15781.